Cellular/Molecular

Processing of Hippocampal Network Activity in the Receiver Network of the Medial Entorhinal Cortex Layer V

Andrei Rozov,[1] Märt Rannap,[1] Franziska Lorenz,[1] Azat Nasretdinov,[2] ⬛Andreas Draguhn,[1] and
⬛Alexei V. Egorov[1]

[1]Institute of Physiology and Pathophysiology, Heidelberg University, 69120 Heidelberg, Germany, and [2]Laboratory of Neurobiology, Kazan Federal University, Kazan 420008, Russia

The interplay between hippocampus and medial entorhinal cortex (mEC) is of key importance for forming spatial representations. Within the hippocampal–entorhinal loop, the hippocampus receives context-specific signals from layers II/III of the mEC and feeds memory-associated activity back into layer V (LV). The processing of this output signal within the mEC, however, is largely unknown. We characterized the activation of the receiving mEC network by evoked and naturally occurring output patterns in mouse hippocampal-entorhinal cortex slices. Both types of glutamatergic neurons (mEC LVa and LVb) as well as fast-spiking inhibitory interneurons receive direct excitatory input from the intermediate/ventral hippocampus. Connections between the two types of excitatory neurons are sparse, and local processing of hippocampal output signals within mEC LV is asymmetric, favoring excitation of far projecting LVa neurons over locally projecting LVb neurons. These findings suggest a new role for mEC LV as a bifurcation gate for feedforward (telencephalic) and feedback (entorhinal–hippocampal) signal propagation.

Key words: layers Va and Vb; local connectivity; medial entorhinal cortex; mouse; postsynaptic currents; sharp wave-ripples

---

Significance Statement

Patterned network activity in hippocampal networks plays a key role in the formation and consolidation of spatial memories. It is, however, largely unclear how information is transferred to the neocortex for long-term engrams. Here, we elucidate the propagation of network activity from the hippocampus to the medial entorhinal cortex. We show that patterned output from the hippocampus reaches both major cell types of deep entorhinal layers. These cells are, however, only weakly connected, giving rise to two parallel streams of activity for local and remote signal propagation, respectively. The relative weight of both pathways is regulated by local inhibitory interneurons. Our data reveal important insights into the hippocampal–neocortical dialogue, which is of key importance for memory consolidation in the mammalian brain.

Introduction

Complex behavioral or cognitive tasks are supported by large-scale functional neuronal systems (Fuster, 2006; Bressler and Menon, 2010). Within this distributed architecture, coordinated activity patterns often propagate along chains or loops of interconnected networks (Kumar et al., 2010). In many cases, such activity patterns are synchronized by coherent network oscillations (Gray and Singer, 1989; Chrobak and Buzsáki, 1996, 1998; Seidenbecher et al., 2003). A prominent example of propagating network oscillations is the hippocampal–entorhinal loop, which plays a key role in spatial representation, navigation, and episodic memory (Buzsáki and Moser, 2013).

The entorhinal cortex (EC) constitutes a major interface between the hippocampus and various regions of the neocortex (van Strien et al., 2009) and is subdivided into a medial (mEC) and a lateral (lEC) area. Multimodal sensory information enters the hippocampal formation via neurons located in superficial layers of the EC (layers II and III). In turn, the deeply located layer V (LV) receives a substantial part of the hippocampal output (Witter et al., 2017). Layer V of the mEC does, therefore, play a key role in transferring transiently stored hippocampal information to long-term engrams in neocortical networks (Squire et al., 2015). This "readout" function takes the form of propagating sharp wave–ripple complexes (SPW-Rs; Buzsáki, 1986, 1989, 2015),

which contain precise representations of previous experience (Siapas and Wilson, 1998; Girardeau et al., 2009; Nakashiba et al., 2009; Khodagholy et al., 2017).

Initially, layer V of the mEC was considered a largely homogeneous cortical micronetwork with morphologically distinct types of principal neurons lacking the following clear functional specializations: pyramidal cells, horizontal cells, and polymorphic cells (Hamam et al., 2000; Egorov et al., 2002; Canto and Witter, 2012). However, recent work in rodents shows that it can be divided into two functionally separate sublayers with differential expression of transcription factors and different circuit integration (Sürmeli et al., 2015; Ohara et al., 2018). Layer Va (LVa) contains Etv1-positive horizontal neurons, which form the major source of telencephalic projections. In contrast, pyramidal-like neurons in layer Vb (LVb) express Ctip2, and their axons reach mostly local targets including superficial layers II and III of the EC, which, in turn, project back to the hippocampus. LVb excitatory cells have been proposed to be the main targets of afferent fibers from CA1 and the subiculum and, at the same time, the main source of excitation of LVa neurons (Sürmeli et al., 2015; Ohara et al., 2018). This organization predicts a central and unique role for locally projecting LVb neurons in hippocampal output processing.

We have measured responses of LVa and LVb neurons as well as fast-spiking (FS) inhibitory neurons in mEC layer V to afferent hippocampal activity in mouse hippocampal-entorhinal brain slices. We report that stimulation-evoked inputs as well as naturally occurring network events (SPW-Rs) directly excite all three types of neurons. Moreover, excitatory connections between both glutamatergic cell types are very sparse, suggesting separation of hippocampal output signals into two distinct excitatory pathways. The strength of excitatory hippocampal input and the balance between local excitatory and inhibitory connections favor activation of telencephalic-projecting LVa over locally projecting LVb neurons and, hence, the open-loop mode required for memory consolidation.

Materials and Methods

Preparation of mouse brain slices. Horizontal brain slices (300–450 μm thick) containing the hippocampus and entorhinal cortex were obtained from male C57BL/6N mice or genetically modified reporter mice [B6.Cg-Gad1tm1Tama (GAD67-GFP) and B6.129P2-Pvalbtm1(cre)Arbr/J x B6.Cg-Gt(ROSA)26Sortm14(CAG-tdTomato)/Hze/J (PV-Cre; tdTomato)] 4–12 weeks of age using standard proceedings (Roth et al., 2016). C57BL/6N mice were purchased from Charles River Laboratories (strain code 027) and were taken care of in the Interfaculty Biomedical Research Facility in Heidelberg. Housing was provided in Makrolon II cages with a maximum of three animals and tissue nesting material made of cellulose. Animals had *ad libitum* access to food and water. All experimental protocols were conducted in compliance with German law and with the approval of the State Government of Baden-Württemberg (Projects T100/15 and G188/15). Mice were killed under deep CO_2-induced anesthesia. After decapitation, brains were rapidly removed and placed in cold (1–4°C) oxygenated artificial CSF (ACSF) containing the following (in mM): 124 NaCl, 3 KCl, 1.6 $CaCl_2$, 1.8 $MgSO_4$, 10 glucose, 1.25 NaH_2PO_4, and 26 $NaHCO_3$, saturated with carbogen (95% O_2 and 5% CO_2), pH 7.4 at 34°C. Horizontal brain slices containing the intermediate/ventral portion of the hippocampus and connected areas of the entorhinal cortex (Fig. 1A) were cut using a vibratome slicer (model VT1200S, Leica). Section level was between approximately −3.7 and −5 mm along the dorsoventral axis. To better preserve connectivity between the hippocampus and entorhinal cortex, slices were cut with an angle of ∼15° toward the ventral side. Thickness of the slices was 450 μm for experiments with registration of SPW-R-associated postsynaptic responses, 350 μm for optogenetic activation of mEC neurons after adeno-associated virus (AAV)-mediated expression of

channelrhodopsin 2 (ChR2) in the dorsal hippocampus, and 300 μm for testing local neuronal connectivity in paired recordings. Before electrophysiological recordings, slices were allowed to recover for at least 2 h. Those slices that were used for the registration of oscillatory activity were transferred into a Haas-type interface chamber (Haas et al., 1979), superfused with ACSF at a rate of 1.5–2 ml/min at 34 ± 1°C. Otherwise, slices were stored in a submerged incubation chamber at room temperature.

Simultaneous recordings of SPW-Rs and postsynaptic responses from LV neurons. After resting in an interface chamber slices were transferred into a modified double perfusion submerged chamber (Hájos et al., 2009) and perfused with ACSF at a rate of 9–10 ml/min at 32 ± 1°C. Extracellular local field potentials (FPs) were recorded from stratum pyramidale of hippocampal area CA1 using ACSF-filled borosilicate glass electrodes (catalog #GB200F-10, Science Products) with a tip diameter of 3–5 μm. Following this protocol, submerged hippocampal slices showed spontaneously occurring SPW-Rs (Maier et al., 2003), which could be reliably observed for at least 2 h. Extracellular FPs were amplified 100× with an EXT 10-2F amplifier (npi electronics). Signals were digitized at 10 kHz with an analog-to-digital converter [ADC; model MICRO 1401 mkII, Cambridge Electronic Design (CED)] and saved on a computer using PATCHMASTER software (HEKA) for offline analysis. Paired patch-clamp recordings were performed using two EPC7 amplifiers (HEKA). Layer V neurons (Va and Vb excitatory cells, and FS interneurons) were identified with an upright microscope (BX-51 WI, Olympus) at 40× magnification using infrared-differential interference contrast (DIC) microscopy and in some cases with subsequent fluorescence microscopy. Whole-cell current-clamp (CC) recordings were performed simultaneously from two layer V neurons using borosilicate glass pipettes with resistances of 5–7 MΩ containing the following (mM): 144 K-gluconate, 4 KCl, 10 HEPES, 4 Mg-ATP, 0.3 Na-GTP, and 10 Na_2-phosphocreatine, adjusted to pH 7.3 with KOH. During recordings, cells were held at resting membrane potential (RMP), unless otherwise indicated. Baseline activity was monitored for at least 15 min in ACSF. For the isolation of monosynaptic responses, an elevated divalent cation (EDC) solution (ACSF containing 4 mM Ca^{2+} and 6 mM Mg^{2+}; McLean et al., 1996; Liao and Walters, 2002) was continuously perfused for at least 20 min. Recordings in EDC solution were performed 10 min after the start of the perfusion. For recordings of postsynaptic currents patch pipettes were filled with a Cs^+-based internal solution, which consisted of the following (in mM): 144 Cs-gluconate, 4 CsCl, 10 HEPES, 4 Mg-ATP, 0.3 Na-GTP, and 10 Na_2-phosphocreatine, adjusted to pH 7.3 with CsOH. Holding membrane potentials in voltage-clamp mode were corrected for the liquid junction potential of approximately −15 mV. During recordings, cells were filled with biocytin (1–5%; catalog #B4261, Sigma-Aldrich) for subsequent morphologic analysis.

Examining connectivity in the mEC layer V network. Dual whole-cell recordings were performed at 32 ± 1°C. Slices were continuously superfused with an extracellular solution containing the following (in mM): 125 NaCl, 2.5 KCl, 25 glucose, 25 $NaHCO_3$, 1.25 NaH_2PO_4, 2 $CaCl_2$, and 1 $MgCl_2$, bubbled with 95% O_2/5% CO_2. The pipette solution contained the following (in mM): 110 K-gluconate, 30 KCl, 8 NaCl, 10 HEPES, 4 Mg-ATP, 0.3 Na-GTP, and 10 Na_2-phosphocreatine, adjusted to pH 7.3 with KOH. In experiments studying SPW-R propagation to LVa and LVb, neuron pairs were recorded with a low-chloride pipette solution containing 4 mM KCl. During experiments, neurons were preliminarily identified at 40× magnification using infrared-DIC microscopy. All cells were filled with biocytin for subsequent morphologic analysis. Those cells that had truncated axons were excluded from connectivity analysis as presynaptic neurons. Presynaptic and postsynaptic neurons were located within ∼150 μm from each other. To study synaptic connections, presynaptic cells were stimulated with a 10 Hz train of five suprathreshold current pulses, which were repeated every 10 s. All paired recordings used for connectivity analysis were conducted in CC mode. During recordings, cells were held at RMP. Averages of 50–100 consecutive sweeps were used for the analysis of postsynaptic responses.

Identification and characteristics of layer V neurons. During experiments layer Va and Vb excitatory neurons were preliminarily identified based on their location and shape of cell body, as previously described
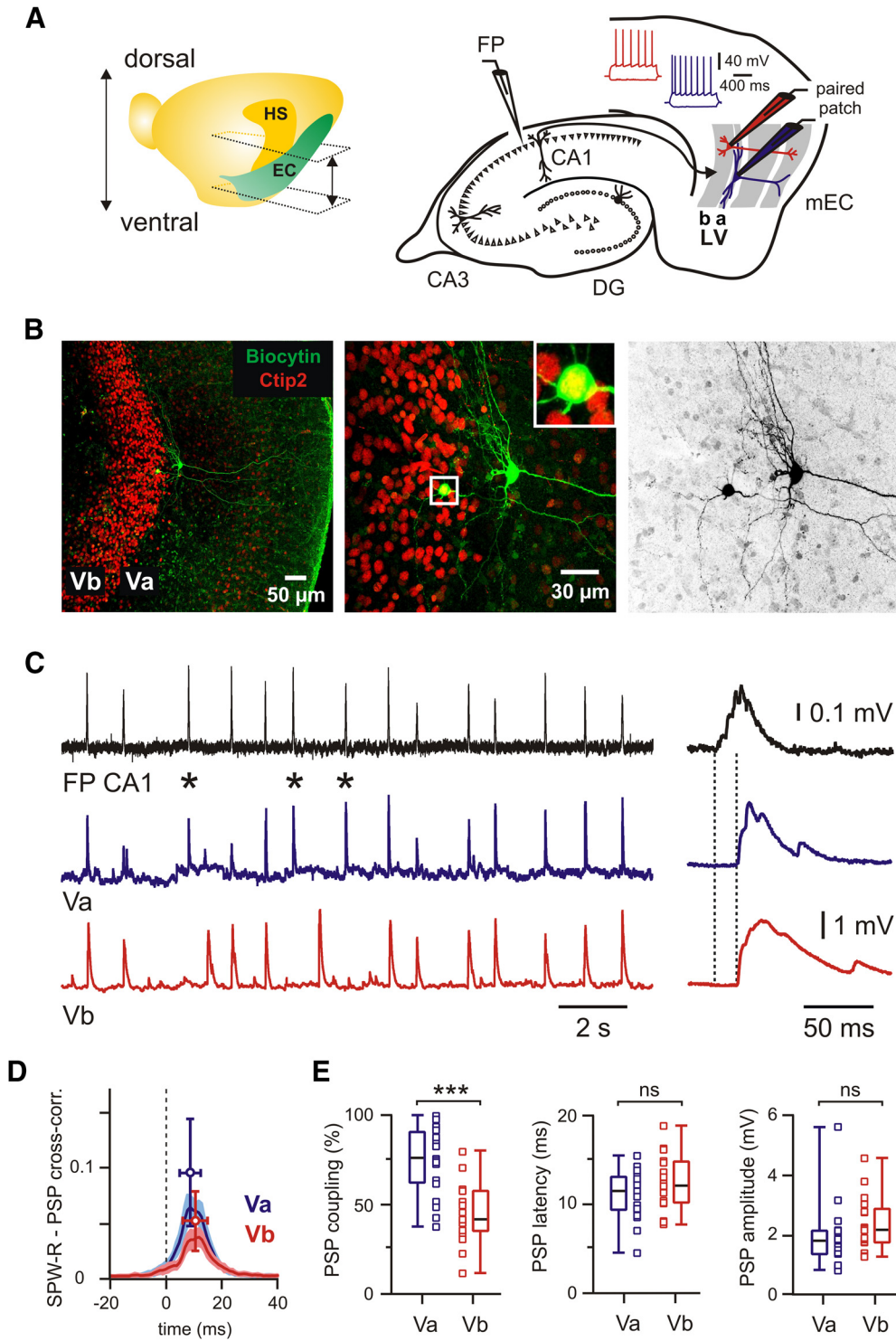
Figure 1. Propagation of SPW-Rs to LVa and LVb excitatory neurons in mEC. **A**, Left, Location of EC and hippocampus (HS) in the left brain hemisphere with approximate positions of horizontal sections used in experiments. Right, Schematic representation of horizontal hippocampal–EC slice with position of FP and patch-clamp electrodes. Insets show intrinsic firing properties of LVa (blue) and LVb (red). **B**, z-Projected confocal images of biocytin-filled mEC LVa and LVb neurons overlaid with Ctip2 immunolabeling (left and middle). Inset (boxed area) shows at higher magnification the Ctip2-positive LVb neuron. Right image shows the same neurons in black and white contrast. **C**, PSPs of excitatory neurons in LVa (blue trace) and LVb (red trace) during spontaneous SPW-Rs in CA1 (FP; black trace). SPW-Rs that induced a PSP in the LVa neuron but failed to trigger a response in the LVb cell are labeled with asterisks. Expanded traces of a single event are shown on the right. Dotted lines indicate PSP latency. **D**, Averaged cross-correlograms between SPW-Rs and PSPs in LVa (blue) and LVb (red) neurons (peak values: mean ± SD). **E**, Box plots show higher PSP coupling to SPW-Rs for LVa compared with LVb neurons and no differences for PSP latency and amplitude. Data are presented as the median (P_{25}; P_{75}) and individual values. Whiskers show minimum and maximum values. Mann–Whitney test: ***$p < 0.001$; ns, not significant.

(Sürmeli et al., 2015), as well as on their firing properties (Fig. 1A). After recordings, morphology, and location were defined following immunostaining of biocytin-filled neurons. Cell location within layer V was further verified by immunolabeling for the transcription factor Ctip2,

which marked neurons in a region corresponding to sublayer Vb (Fig. 1B). All LVb neurons ($n = 169$) had a morphology of pyramidal cells with basal dendrites primarily restricted within the layer (Sürmeli et al., 2015). The vast majority of LVb pyramidal neurons (93% from 114

verified cells) were immunopositive for Ctip2 (Sürmeli et al., 2015; Ohara et al., 2018). In contrast, LVa neurons displayed a characteristic horizontal basal dendritic tree located in a narrow zone of layer V adjacent to lamina dissecans and were commonly immunonegative for Ctip2 (only 6 of 146 stained LVa cells showed strong immunoreactivity for Ctip2). The majority of LVa horizontal neurons had a large apical dendrite extending toward superficial layers of the mEC (127 of 154, corresponding to 82%). The remaining 18% were nonpyramidal horizontal cells lacking this apical dendrite.

Resting membrane potential in CC mode was estimated as baseline potential without current injection and without correction for liquid junction potential. Input resistance (IR) was determined at RMP by passing negative current pulses (−50 pA, 1 s) through the recording electrode and measuring the resulting voltage deflections (at a late steady-state level). In recordings with 4 mM KCl in the pipette solution, the RMP of LVa neurons was −62 mV [median; 25th percentile (P_{25}) = −61, 75th percentile (P_{75}) = −65; $n = 57$] and the IR was 121 MΩ (median; $P_{25} = 98$, $P_{75} = 160$; $n = 56$). For LVb neurons, the RMP was −70 mV (median; −68, −72; $n = 64$) and the IR was 178 MΩ (median; 148, 222; $n = 64$; LVa vs LVb: $p < 0.0001$ for both parameters, Mann–Whitney test). For recordings with 30 mM KCl in the pipette solution, the RMP of LVa neurons was −68 mV (median; −65, −69; $n = 43$) and the IR was 140 MΩ (median; 116, 182; $n = 43$). Values of LVb neurons were −71 mV (median; −70, −73; $n = 81$) and 156 MΩ (median; 132, 192; $n = 79$), respectively (LVa vs LVb: $p < 0.0001$ for RMP, $p = 0.201$ for IR, Mann–Whitney test). FS interneurons were recorded in slices obtained from C57BL/6N mice or genetically modified reporter mice (see below). Cells were identified based on their characteristic firing properties (see Fig. 4E). All interneurons were located within layer V (including both LVa and LVb) as confirmed through immunostaining of biocytin-filled cells. The median RMP of FS interneurons was −75 mV (−68, −78; $n = 21$) and median IR was 121 MΩ (102, 143; $n = 21$) for a pipette solution containing 4 mM KCl. For recordings with 30 mM KCl RMP and IR were −77 mV (−73, −79; $n = 44$) and 127 MΩ (103, 157; $n = 42$), respectively.

Electrical stimulation. An extracellular bipolar platinum/iridium electrode (75 µm tip separation; impedance, 0.1 MΩ; catalog #PI2ST30.1A3, MicroProbes) was used to evoke synaptic responses in the mEC by local stimulation of the alveus in CA1. Pulses (0.1 ms, 2–10 V) were delivered with a constant voltage isolator stimulator (model DS2A-Mk.II, Digitimer). Stimulation artifacts were trimmed in original traces shown in figures.

Injection of virus and optogenetic stimulation. All experiments requiring injections of AAV vectors were conducted in a biosafety level 2 laboratory. Subcutaneous injections of buprenorphine (0.1 mg/kg) were administered 30 min before and 3 h after each operation. During operations, mice were deeply anesthetized with isoflurane (4%) and mounted in a stereotaxic frame. Anesthesia was maintained by mask inhalation of vaporized isoflurane at concentrations between 1.5% and 2.5%. Following head fixation, the skull was exposed and a small burr hole was drilled above the injection site. The injection was made by means of a stainless steel needle (NF33BV; inner tip diameter, 115 µm) connected to a 10 µl NanoFil Syringe (World Precision Instruments). Coordinates of injection sites were based on the mouse brain atlas (Paxinos and Franklin, 2001) and calculated from bregma. Mice received injections of 200–300 nl AAV5-CaMKIIa-hChR2(H134R)-EYFP (UNC Vector Core, Karl Deisseroth virus stock) into the intermediate/ventral hippocampus [anteroposterior (AP), −3.2 to 3.4 mm; mediolateral (ML), ±3.4 to 3.55 mm; dorsoventral (DV), −3.6 to 4.0 mm] or 70–200 nl into the dorsal hippocampus [AP, −2 mm; ML, ±2 mm; DV, −1.5 mm (13 mice); or AP, −1.5 mm; ML, ±1.2 mm; DV, −1.4 mm (5 mice)] at a rate of 200 nl/min. The needle was left in place for another 10 min before it was withdrawn. When all injections were completed, the wound was sutured and the animal was monitored during recovery from anesthesia, after which it was returned to its home cage. Animals were allowed to recover for a minimum of 2 weeks after injections, before being sacrificed. Hippocampal pyramidal cells or their axonal fibers expressing ChR2 were excited through a 40×/0.8 numerical aperture (NA) objective using a transistor–transistor logic-controlled blue LED (470 nm; pulses,

1–5 ms; catalog #M470L3, ThorLabs). Neurons in the mEC were recorded in CC mode at a membrane potential of approximately −70 mV using the K gluconate-based pipette solution containing 4 mM KCl (see above). Responses to optogenetic activation of axonal projections from the dorsal hippocampal CA1 area were measured using an ELC-03XS amplifier (npi electronics) connected to an ADC (POWER 1401 mkII, CED), and Signal4 and Spike2 (version 7) software (CED). Because no significant differences in synaptic responses between the two dorsal hippocampal injection locations were detected, data from both groups were pooled.

Immunohistochemistry and confocal microscopy. Slices containing cells filled with biocytin were fixed in 4% paraformaldehyde in phosphate buffer (PB) for 90 min at room temperature, and then kept in PBS, pH 7.4 at 4°C. Before the application of primary antibodies, slices were pretreated in blocking solution (5% goat serum and 0.3% Triton X-100 in PBS) for 2 h at room temperature. Next, slices were washed in PBS (3-× 15 min) and incubated overnight (>16 h at room temperature) with primary antibodies (rat anti-Ctip2; 1:1000; catalog #ab18465, Abcam) diluted in antibody solution (1% goat serum and 0.2% Triton X-100 in PBS). After overnight incubation slices were washed in PBS (3 -× 15 min) and transferred to a secondary antibody solution for 2 h at room temperature. The following secondary antibodies were used: Alexa Fluor 488 anti-rat (1:1000; catalog #A11006, Thermo Fisher Scientific), Avidin Alexa Fluor 488 conjugate (1:1000; catalog #A21370, Thermo Fisher Scientific), Cy3-conjugated anti-rat (1:500; 112–165-003, Jackson ImmunoResearch), streptavidin-conjugated Alexa Fluor 546 (1:1000; catalog #S11225, Thermo Fisher Scientific), and Alexa Fluor 647 anti-rat (1:1000; A21247, Thermo Fisher Scientific). All secondary antibodies were diluted in antibody buffer (1% goat serum and 0.2% Triton X-100 in PBS). Slices were then washed in PBS (3× 15 min) and incubated with DAPI (1:10,000; Carl Roth) for 2 min at room temperature. Slices were subsequently washed in PBS (15 min) and embedded in Mowiol 4-88 (Sigma-Aldrich). Confocal image stacks were collected with an A1R or C2 Nikon confocal microscope (Nikon Imaging Center at Heidelberg University) at 1024 × 1024 pixel resolution (1 µm z-steps) using 4× (0.13 NA) or 20× (0.75 NA) objectives in air or a 60× (1.4 NA) oil-immersion objective. Multiple confocal images were merged as maximum intensity projections and analyzed in ImageJ/Fiji (Wayne Rasband, NIH, open source). Distances between neurons were calculated in XY dimension from the center of the soma using ImageJ. Values were then corrected for the z-axis to obtain the distance in three dimensions.

Data analysis. Raw data were digitally filtered using the RC (resistor–capacitor) filter routine of MATLAB [bandpass: 1–80 Hz for SPW-Rs; 1–500 Hz for postsynaptic potentials (PSPs); and 0.1–500 Hz for postsynaptic currents (PSCs)]. For signal detection, a two-threshold method was applied as follows. First, events exceeding three SDs of the full-length recording were considered as SPW-Rs, PSPs, or PSCs, respectively. Second, approximate onsets and offsets of the SPW-R events were defined as times when the signal intersected a threshold of 1.5 SDs. Exact SPW-R onset was defined as the time when the first derivative of the FP (low-pass filtered at 40 Hz) reached a threshold of 0.02 mV/ms. For PSP detection, approximate onsets and offsets of the signals were defined as the time when the signal intersected a threshold of 1 SD. Exact PSP onset was defined as the time when the first signal derivative (low-pass filtered 500 Hz) reached a threshold of 0.1 mV/ms. For PSCs, approximate onsets and offsets were defined as times when signal intersected a threshold of 0.5 SDs. Exact PSC onset was defined as the time when the first signal derivative (low-pass filtered at 500 Hz) reached a threshold of 10 pA/ms. The correlation between SPW-Rs and PSPs or PSCs was calculated based on cross-correlograms of onsets. The z-scores for cross-correlograms were calculated as previously described (Valeeva et al., 2019). Event duration was calculated as the time between onset and approximate offset (return to baseline levels). Event amplitudes were estimated as the maximum value between onset and approximate offset with subtraction of baseline level (median value from a 3 ms window before onset). Event half-width was estimated as the duration at the half-amplitude level. Latencies between SPW-Rs in CA1 and PSPs/PSCs
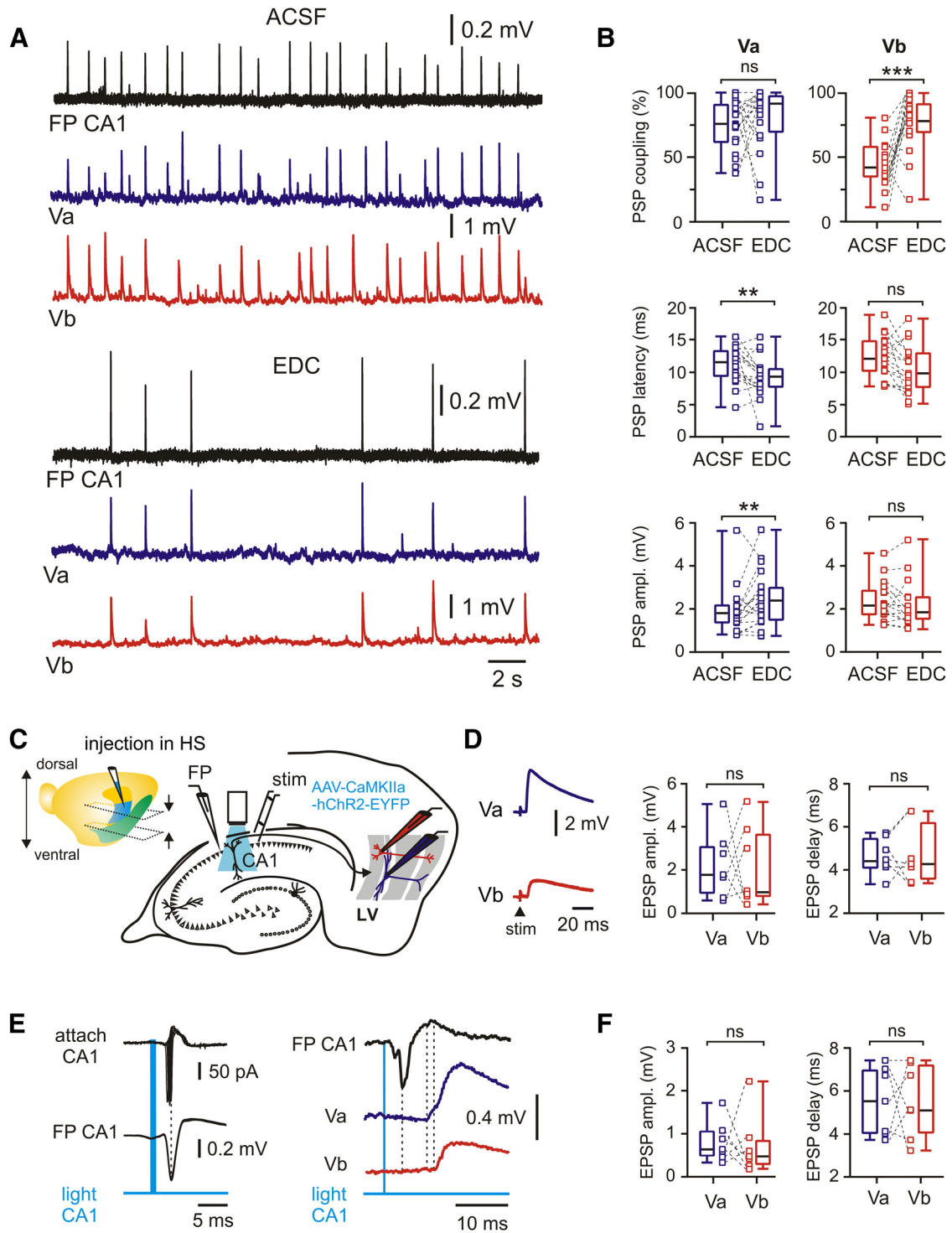
Figure 2. Monosynaptic functional connectivity between CA1 and mEC LVa and LVb neurons. *A*, Spontaneous SPW-Rs in CA1 and associated PSPs in mEC LVa and LVb neurons under control conditions (ACSF) and after isolation of monosynaptic responses with EDC solution. *B*, Box plots show the effects of ACSF substitution with EDC on PSP coupling, PSP latency, and PSP amplitude for LVa and LVb neurons. *C*, Left, Brain hemisphere with indication of injection site in the hippocampal region (HS). Approximate positions of horizontal sections used in experiments are indicated by arrows. Right, Schematic diagram of recording configuration for electrical and optogenetic stimulation of postsynaptic responses in mEC neurons. *D*, Left, Example traces of excitatory postsynaptic responses from a pair of LVa and LVb neurons following electrical stimulation of the alveus. Right, Box plots of EPSP time delay and EPSP amplitude. *E*, Left, Cell-attached recording from a CA1 neuron expressing ChR2 (top) and local FP (middle). Light pulse reliably evokes action potentials and population spikes, respectively. Right, Light-evoked EPSPs recorded from a pair of LVa and LVb neurons. *F*, Box plots of EPSP time delay and EPSP amplitude induced by optogenetic stimulation. All data are presented as the median (P$_{25}$; P$_{75}$). Whiskers show minimum and maximum values. Connected squares represent individual values. Wilcoxon test: **$p < 0.01$; ***$p < 0.001$; ns, not significant.

in the mEC were defined as the time interval between onset of field-SPW-R and onset of postsynaptic events. PSPs or PSCs in the mEC were considered SPW-R driven if their onset time was <50 ms following the beginning of an SPW-R event in CA1. For PSP peak detection, the signal was additionally filtered by a 20 Hz high-pass RC filter, and events exceeding 1.5 SDs of the filtered signal were considered as unitary responses in compound PSPs or PSCs. All data were analyzed offline using PatchMaster (HEKA), SigmaPlot (Systat) and MATLAB R2012 (MathWorks). Values of EPSP/PSP amplitudes of connected pairs were calculated from averaged first synaptic responses in trains of 5.

Statistical analysis. Quantitative data from multiple slices are given as the median (P_{25}; P_{75}). Data in figures are presented as medians (P_{25}; P_{75}) and individual values. Whiskers show minimum and maximum values. For values shown in figures, data in main text are given just as the median. Statistical analysis was performed using SigmaPlot (Systat) or Graph Pad (InStat, GraphPad Software). Mann–Whitney *U test*, Wilcoxon Rank Sum test or Fisher's exact test were used for statistical comparisons as indicated in the text. A *p* value <0.05 was regarded as significant (for all data: *p < 0.05, **p < 0.01, ***p < 0.001, ns, not significant). Regression analysis was performed using simple linear regression or exponential curve fitting in MATLAB (curve-fitting toolbox), quantified by the correlation coefficient r^2.

Results

Propagation of SPW-Rs to LVa and LVb excitatory neurons in mEC

The deep layers of the mEC are an important target for excitatory input from the hippocampus, but many details about signal propagation between both networks remain unclear. We recorded a naturally occurring hippocampal activity pattern, SPW-Rs, in mouse horizontal slices containing both the intermediate/ventral hippocampus and the entorhinal cortex (Fig. 1A). SPW-Rs were recorded as field potentials in CA1 stratum pyramidale concurrently with paired whole-cell recordings of identified mEC LVa and LVb excitatory neurons (Fig. 1A,B; see Materials and Methods). SPW-Rs propagated efficiently to both cell populations, causing well discernible compound PSPs (Fig. 1C). Coupling of postsynaptic potentials to the afferent network activity was confirmed by cross-correlation analysis (Fig. 1D), which yielded high *z*-score values for both cell types [LVa: median, 45.5 (P_{25} = 35.4; P_{75} = 65.7); LVb: 30.9 (P_{25} = 19.6; P_{75} = 39.5)]. Peak values of cross-correlograms were higher for LVa neurons compared with LVb neurons (*p* = 0.009, Mann–Whitney test). Similarly, PSP coupling, measured as the percentage of SPW-Rs followed by PSPs in the recorded cell, was significantly higher in LVa (median, 76%; *n* = 19) when compared with LVb neurons (median, 42%; *n* = 17; *p* = 0.0001, Mann–Whitney test; 14 mice; 16 paired recordings; Fig. 1E). In contrast, latencies between SPW-Rs in CA1 and PSPs in the mEC were similar between LVa (11.6 ms,
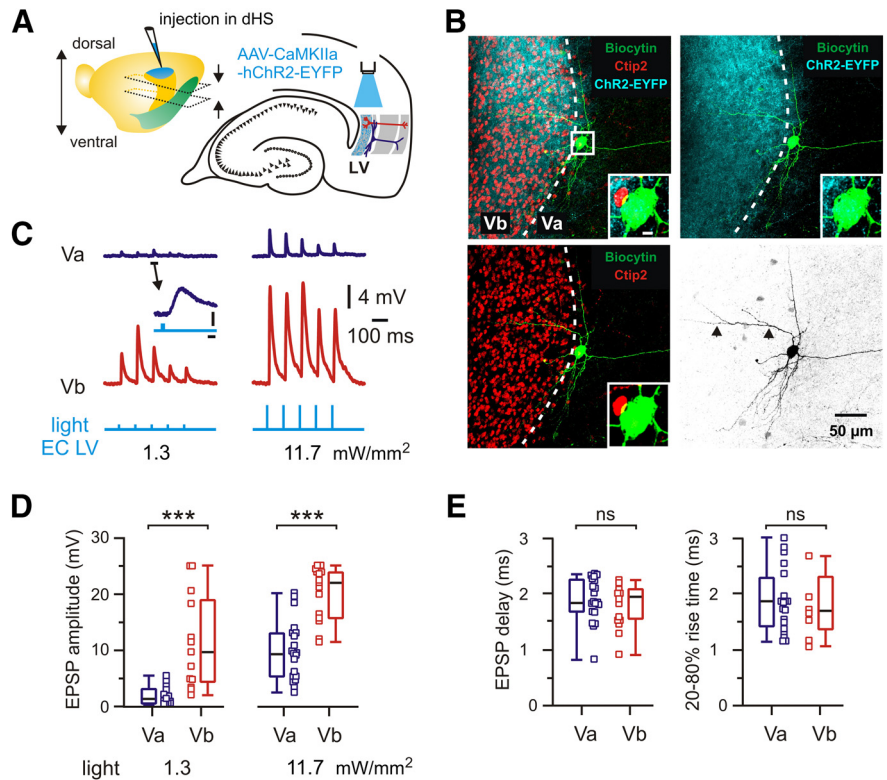

Figure 3. Functional connectivity between dorsal hippocampus and mEC LVa and LVb excitatory neurons. *A*, Left, Brain hemisphere with indication of the injection site in the dorsal hippocampus (dHS). Approximate positions of horizontal sections used in experiments are indicated by arrows. Note the more dorsal location of slices. Right, Schematic representation of horizontal hippocampal–EC slice with position of light stimulation to activate axons from dorsal hippocampal neurons infected with AAV-CaMKIIa-hChR2-EYFP. *B*, z-Projected confocal images of a biocytin-filled mEC LVa neuron overlaid with Ctip2 immunolabeling and fluorescent staining of hippocampal axons expressing hChR2-EYFP. Dotted line indicates the approximate border between LVb and LVa. Note the strong fluorescence of axonal fibers in Ctip2-positive LVb and weak but recognizable fluorescence around the Ctip2-negative LVa neuron. Insets, Higher magnification of the soma indicated by boxed area. Scale bar, 5 μm. Right bottom image shows the same neuron in black and white contrast. A dendritic branch extending within LVb is indicated by arrowheads. *C*, Light-evoked EPSPs recorded from LVa and LVb neurons. Example traces of synaptic responses corresponding to two different stimulation intensities. Note that low-intensity light pulses do trigger clearly discernible synaptic responses in the LVa neuron. The marked event is shown at expanded scale. Calibration: 2 ms, 0.5 mV. Blue light pulses, 1 ms. *D*, Box plots of EPSP amplitude induced by light pulses with two different stimulation intensities. *E*, Box plots of EPSP time delay and EPSP 20–80% rise time. Data obtained from recordings with 11.7 mW/mm² light pulse intensity. All data are presented as the median (P_{25}; P_{75}). Whiskers show minimum and maximum values. Squares represent individual values. Mann–Whitney test: ***p < 0.001; ns, not significant.

n = 19) and LVb (12.1 ms, *n* = 17) cells (*p* = 0.342, Mann–Whitney test). Median values of SPW-R driven PSP amplitudes were also not significantly different (LVa: 1.8 mV, *n* = 19; LVb: 2.2 mV, *n* = 17; *p* = 0.099, Mann–Whitney test; Fig. 1E). Finally, we compared the half-width of SPW-R-coupled PSPs [LVa: 23.5 ms (19.3; 28.5); LVb: 25.0 ms (19.1; 33.9)] and the number of peaks in the compound signals [LVa: 3.2 (2.7; 3.3), LVb: 2.8 (2.5; 3.4)]. These waveform-related parameters were also similar between both cell populations (LVa vs LVb: *p* = 0.506 for half-width, *p* = 0.59 for number of peaks, Mann–Whitney test).

We next tested whether SPW-R propagation to both deep sublayers of the mEC was preferentially mediated by monosynaptic connections. We made use of an extracellular solution with EDCs that strongly reduces polysynaptic signals (McLean et al., 1996; Liao and Walters, 2002). Switching from ACSF to EDC led to a drastic reduction of SPW-R frequency [ACSF: 80 events/min (63; 95); EDC: 15 events/min (9; 22); *n* = 19; *p* < 0.0001, Wilcoxon test], while the amplitude of the events significantly increased [ACSF: 0.17 mV (0.12; 0.22); EDC: 0.38 mV (0.24; 0.49); *n* = 19; *p* = 0.001, Wilcoxon test; Fig. 2A]. Postsynaptic
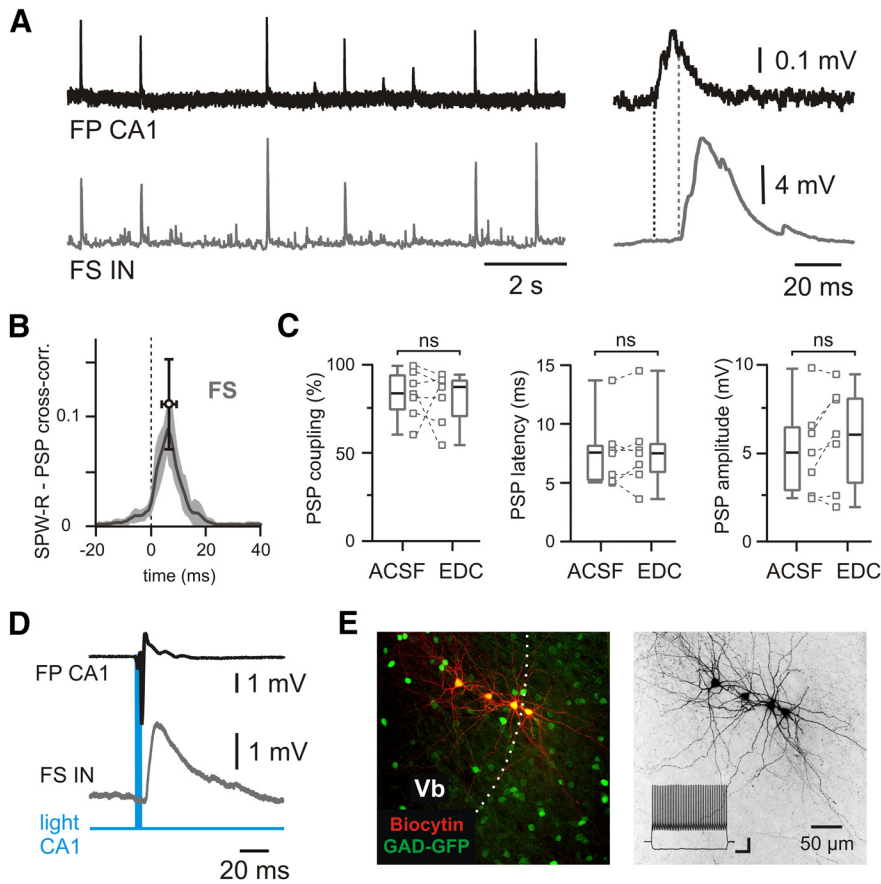
A

B

C

D

E

Figure 4. Propagation of SPW-Rs to mEC LV fast-spiking interneurons. **A**, PSPs of an FS interneuron (bottom trace) during spontaneous SPW-Rs in CA1 (top trace). Expanded traces of a single event are shown on the right. Dotted lines indicate PSP latency. **B**, Averaged cross-correlograms between SPW-Rs and PSPs in FS interneurons (peak values: mean ± SD; n = 7). **C**, Box plots of PSP coupling, PSP latency, and PSP amplitude for FS interneurons recorded in normal ACSF and in EDC solution (monosynaptic responses). Data are presented as the median (P$_{25}$; P$_{75}$) and individual values. Whiskers show minimum and maximum values. Wilcoxon test: ns, not significant. **D**, Example of light-evoked field potential response in CA1 followed by an EPSP in an mEC LV FS interneuron. **E**, z-Projected confocal image of biocytin-filled mEC LV FS interneurons recorded in GAD-GFP mouse (left). Dotted line indicates the approximate border between LVb and LVa. Right image shows the same neurons in black and white contrast. Responses of LV FS interneuron to injected current steps are shown in the inset. Calibration: 200 ms, 10 mV.

responses in layer Va and layer Vb of the mEC changed in several aspects: success rate of SPW-R propagation to LVb pyramidal cells increased from 42% to 78% (n = 17; p = 0.0008, Wilcoxon test), while an apparent increase from 76% to 92% in LVa neurons was not significant (n = 19; p = 0.246, Wilcoxon test; Fig. 2B). Latencies between hippocampal SPW-Rs and postsynaptic potentials became shorter in both sublayers (ACSF to EDC; LVa: 11.6 to 9.2 ms; n = 19; p = 0.009; LVb: 12.1 to 9.9 ms; n = 17; p = 0.051; Wilcoxon test; Fig. 2B). In LVa neurons, amplitudes of SPW-R-triggered PSPs increased significantly (1.8 to 2.4 mV; n = 19; p = 0.009, Wilcoxon test), while they remained unchanged in LVb cells (2.2 to 1.8 mV; n = 17; p = 0.174, Wilcoxon test). Finally, PSP waveforms became less complex: half-width was reduced in the "monosynaptic" solution (LVa: 23.5 to 18.5 ms [16; 20.8]; LVb: 25.0 to 15.5 ms [13.8; 19.7]; p < 0.0001 for both, Wilcoxon test) and postsynaptic potentials showed less discernible peaks in LVb pyramidal cells [2.8 to 2.6 (2.0; 2.8) per response; p = 0.013, Wilcoxon test]. This number stayed constant in layer Va neurons [3.2 to 3.1 (2.5; 3.6); p = 0.395, Wilcoxon test]. Together, these data suggest a strong monosynaptic component in the pathways for hippocampal SPW-R propagation from CA1 to both LVa and LVb neurons.

Furthermore, LVa cells responded to hippocampal network events more reliably than LVb neurons.

Direct hippocampal input to LVa and LVb excitatory neurons in mEC

For a quantitative assessment of the functional connectivity between intermediate/ventral hippocampus and deep layers of the mEC, we activated hippocampal afferents by electrical or optogenetic stimulation (all in ACSF; Fig. 2C). In the first series of experiments, a bipolar stimulation electrode was placed in the alveus of CA1. Stimulus strength was set to trigger reliable postsynaptic responses in LVb cells with amplitudes between 1 and 4 mV (Roth et al., 2016). Cells were held at a membrane potential of approximately −70 mV with the internal solution containing 4 mM KCl (calculated E$_{GABA-A}$ − 92 mV) such that depolarizing potentials were exclusively excitatory (EPSPs). Under these conditions, evoked EPSPs had similar amplitudes in both LVa and LVb neurons (median value in LVa: 1.8 mV; LVb: 1.0 mV; n = 7; p = 0.938, Wilcoxon test; Fig. 2D). Moreover, delay times between stimulus artifact and onset of EPSPs were nearly the same in both cell populations (LVa: 4.4 ms; LVb: 4.3 ms; n = 7, p = 0.844, Wilcoxon test; Fig. 2D). Extracellular electrical stimulation in the alveus may activate axons from diverse cell populations outside CA1. To minimize such contamination, we next expressed ChR2 in CA1 pyramidal cells (see Materials and Methods). Blue light pulses (1–5 ms) reliably triggered spikes in CA1 pyramidal neurons, as shown by juxtacellular recordings. Maximal spiking probability in these neurons was coincident with the negative peak of the nearby measured local FP (n = 5; Fig. 2E, left). Both types of excitatory neurons of mEC layer V responded reliably to the optogenetic activation of CA1 pyramids (Fig. 2E, right). No differences were found in EPSP amplitudes (median values: LVa: 0.62 mV; LVb: 0.45 mV; n = 7; p = 0.687, Wilcoxon test) or delay times relative to the peak of the hippocampal FP (LVa: 5.5 ms; LVb: 5.1 ms; n = 7; p = 0.937, Wilcoxon test; Fig. 2F).

Functional connectivity between dorsal hippocampus and mEC LVa and LVb excitatory neurons

A previous study on brain slices reported that optogenetic activation of dorsal hippocampal afferents failed to elicit responses in LVa neurons while robustly activating LVb neurons (Sürmeli et al., 2015). In apparent contrast, we found reliable responses of both LVa and LVb neurons on stimulation of intermediate/ventral parts of the hippocampus. We tested whether this discrepancy might be explained by differences between dorsal and ventral/intermediate hippocampal–entorhinal projections. For this, we injected an AAV expressing hChR2-EYFP into the dorsal hippocampal CA1 area (Fig. 3; see Materials and Methods).

In horizontal slices at the level of the mEC, dorsal hippocampal neurons are not preserved, such that we directly activated ChR2-expressing hippocampal axons by illuminating LV with blue light (Fig. 3A). Similar to the observations of Sürmeli et al. (2015), a strong fluorescent band of hippocampal axonal fibers was detected along the Ctip2-positive layer Vb, together with a smaller number of individual fibers extending toward layer Va (Fig. 3B). We then evaluated the functional responses of 31 LVa and 15 LVb neurons (18 mice) to light stimulation (Fig. 3C–E). All 15 LVb neurons showed strong excitatory potentials following light pulses with a median delay of 1.9 ms ($n = 15$), confirming reliable monosynaptic input from the dorsal hippocampus.

Unexpectedly, 20 of 31 LVa cells likewise responded to light stimulation with short delay times (median, 1.83 ms; $n = 20$), comparable to LVb ($p = 0.386$, Mann–Whitney test; Fig. 3E), suggesting monosynaptic input to these cells. As the 20–80% EPSP rise time was similar between both neurons (LVa: 1.84 ms; $n = 19$; LVb: 1.68 ms; $n = 8$; $p = 0.690$, Mann–Whitney test; Fig. 3E), it is unlikely that indirect effects like glutamate spillover from synapses on LVb cells to neighboring LVa cell dendrites could have caused the detected responses. Synaptic potentials, however, were significantly weaker in LVa neurons compared with LVb neurons. At a low stimulation intensity (1.3 mW/mm^2) the difference in median amplitude was approximately sixfold (LVa: 1.5 mV; $n = 13$, LVb: 9.7 mV; $n = 13$; $p = 0.0002$, Mann–Whitney test). Responses were still strongly different at high intensity (11.7 mW/mm^2; median amplitude: LVa: 9.5 mV, $n = 20$; LVb: 21.9 mV, $n = 15$; $p = 0.0001$; Mann–Whitney test; Fig. 3C,D). The stronger pulses evoked action potentials in 1 of 20 LVa cells, compared with 7 of 15 LVb neurons. Three LVa neurons showed no discernible response to presynaptic stimulation and the remaining 8 of 31 neurons showed responses with a median delay of 3.6 ms (3.3; 4.0), a 20–80% EPSP rise time of 2.7 ms (1.8; 2.9), and an amplitude of 4.0 mV (2.2; 13.2; $n = 8$; 5 mice; values for light intensity 11.7 mW/mm^2), suggesting polysynaptic input to these cells. To validate delay times for polysynaptic connections, we recorded from mEC LIII neurons (identified by biocytin staining), which apparently receive no direct projections from the hippocampus (Nilssen et al., 2019). Synaptic responses had a median delay time of 4.7 ms (4.5; 5.3), an EPSP rise time of 2.1 ms (1.9; 2.3), and an amplitude of 12.2 mV (6.6; 13.6; $n = 7$ for all values; light intensity 11.7 mW/mm^2; 5 mice). Together, these data show that the majority of LVa cells (~65%) do receive monosynaptic input from the dorsal hippocampus. This input is, however, markedly weaker for LVa than for LVb neurons, supporting the previously reported prevalence for LVb (Sürmeli et al., 2015).

Propagation of SPW-Rs to mEC LV fast-spiking interneurons

Ordered activity patterns in neuronal networks depend on the balanced activation of excitatory and inhibitory neurons. We therefore tested whether interneurons in layer V of the mEC receive synaptic input from propagating SPW-Rs (Figs. 4, 5). We recorded from 5 low-threshold spiking (LTS) interneurons and
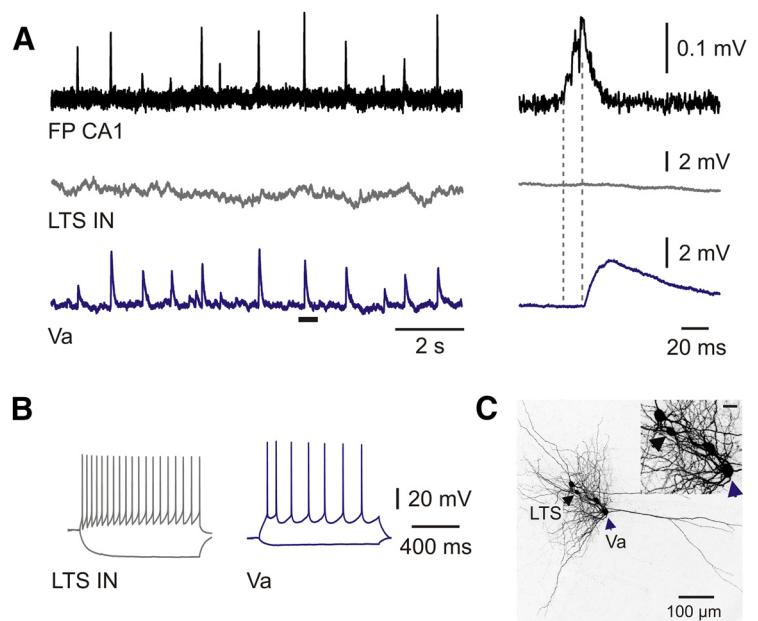

Figure 5. Propagation failure of SPW-Rs to mEC LV LTS interneurons. **A**, Postsynaptic potentials of LV LTS interneuron (gray trace) and LVa horizontal neuron (blue trace) during spontaneous SPW-Rs in CA1 (FP; black trace). Expanded traces of a single event marked by the horizontal bar are shown on the right. Dotted lines indicate PSP latency of the LVa neuron. Note that the SPW-R event failed to trigger a response in the LTS interneuron. **B**, Responses of neurons shown in **A** to injected current steps. **C**, z-Projected confocal image of biocytin-filled mEC LV LTS interneuron and LVa neuron displayed in **A**. Cell bodies are indicated by arrowheads. Inset shows the distance between neurons at higher magnification. Scale bar, 20 μm.

10 FS cells. While none of the LTS cells showed any synchronized activity with SPW-Rs (Fig. 5), the events triggered PSPs in 7 of 10 FS interneurons (Fig. 4A,E). Cross-correlation analysis showed strong coupling of these FS cells to SPW-Rs (Fig. 4B), with a z-score value of 49.9 (45.3; 79.1; $n = 7$). In these cells, SPW-R propagation success was between 61% and 100% (median, 84%; Fig. 4C), close to values obtained for LVa neurons. Synaptic responses in FS cells were delayed by 7.5 ms relative to SPW-R onset (Fig. 4C). Median values for amplitudes and half-width of SPW-R-driven PSPs in FS interneurons were 5 mV (2.9; 6.5) and 14.8 ms (9.8; 15.5), respectively. Most of the responses had multiple peaks [median, 2.5 (2.3; 2.6)]. Substitution of ACSF with the solution favoring monosynaptic responses (EDC) had no significant effect on any of these parameters (Fig. 4C), indicating a monosynaptic SPW-R-related input to FS interneurons. In a separate set of experiments, we tested whether optogenetic stimulation of hippocampal pyramidal cells evokes EPSPs in mEC LV FS interneurons. For this experiment, ChR2 was expressed in hippocampal areas CA1/CA2 in transgenic mice expressing tdTomato in parvalbumin-positive neurons. Similar to layer V excitatory cells, blue light stimulation of CA1 stratum pyramidale caused depolarizing responses in FS interneurons with a characteristic delay of 4.6 ms (4.2; 7.3) and an amplitude of 2.4 mV (2.2; 3.2; $n = 9$; Fig. 3D). These data show a robust feedforward excitation of fast-spiking interneurons of mEC layer V by hippocampal SPW-Rs.

Local connectivity within mEC layer V

Our findings show that hippocampal SPW-Rs reliably propagate to excitatory neurons in LVa and LVb as well as to FS interneurons. Subsequent signal processing within the mEC depends critically on the neuronal interactions within layer V. We therefore studied connectivity between these three types of neurons (Fig.
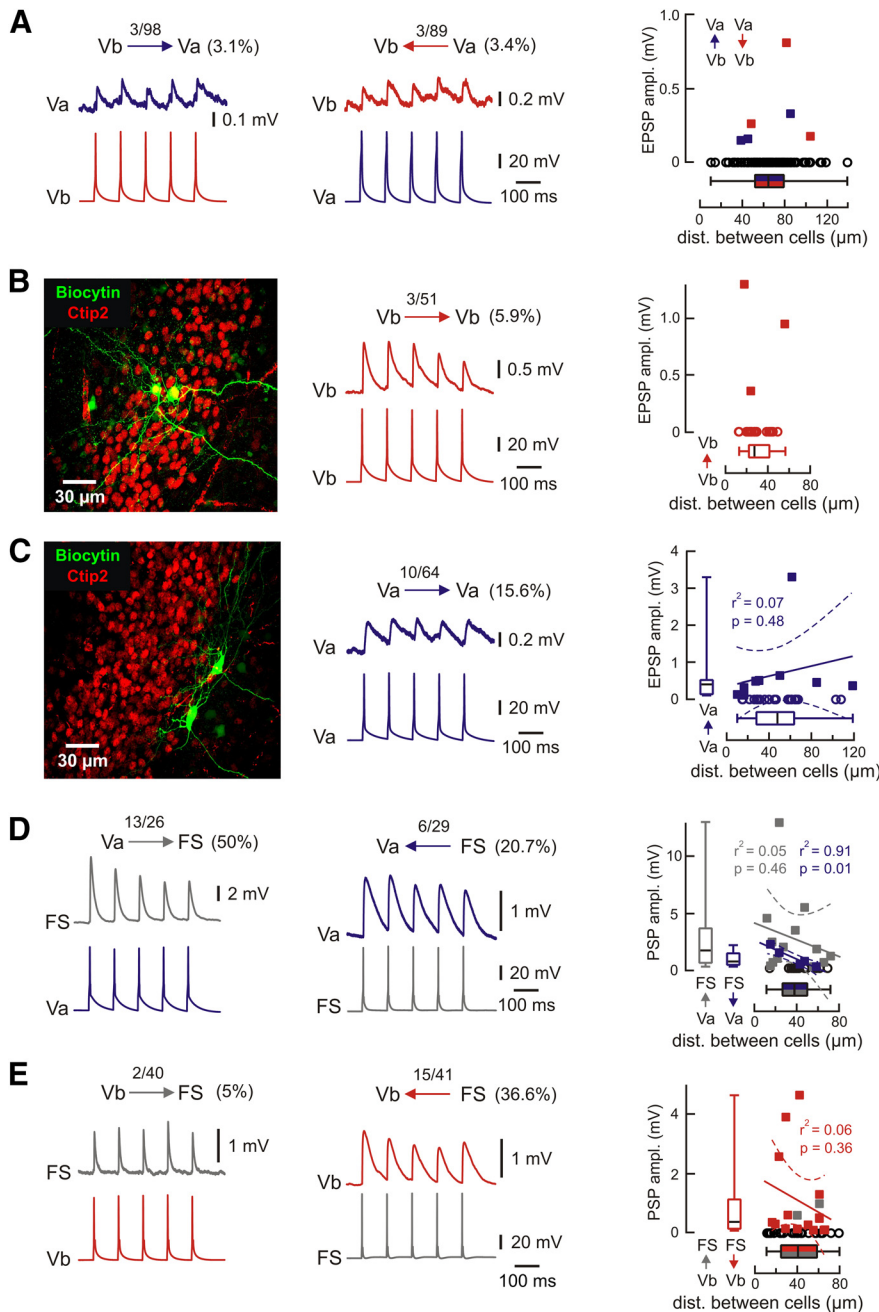
Figure 6. Local connectivity within mEC layer V. **A**, Example traces of paired recordings from pairs of LV neurons showing mutual connectivity between Va and Vb. Numbers indicate the fraction of connected neurons/number of recorded pairs. EPSP amplitudes for connections from layer Vb to Va (blue) and Va to Vb (red) relative to the distance between recorded neurons (right). Open black circles indicate the distance between all tested pairs (note the large number of nonconnected pairs). **B**, Reciprocal connectivity between LVb neurons. Left, z-Projected confocal image of recorded LVb neurons overlaid with Ctip2 immunolabeling. Middle, Example pairs of traces show the presynaptic APs and associated EPSPs recorded from the connected LVb neurons. Right, Values of EPSP amplitude of reciprocally connected pairs within LVb neurons. **C**, Reciprocal connectivity between LVa neurons. The z-projected confocal image for connected LVa neurons (left) and respective example traces (middle). Right, Values of EPSP amplitude of reciprocally connected pairs within LVa neurons. Data are shown relative to distance between neurons. Open circles indicate the distance between all tested pairs including nonconnected cells. Correlation analysis for layer Va neurons shows no significant dependence of connectivity from distance. **D, E**, Example traces showing synaptic connections between pairs of LVa cells and FS interneurons (**D**) and LVb cells and FS interneurons (**E**). Recordings were done with 30 mM chloride intracellular solution to improve the signal-to-noise ratio. Right panels show PSP amplitude relative to the distance between recorded neurons. Open black circles indicate the distance between measured but not connected pairs. Box plots show corresponding medians (P_{25}; P_{75}). Whiskers show minimum and maximum values. Lines show linear regression, and dotted lines indicate 95% confidence interval. Example traces in the figure represent averages of ∼50 subsequent sweeps.

6). We first tested potential connections between the two types of excitatory neurons. Recent transsynaptic tracing experiments indicate a major projection from LVb to LVa neurons, which form the hippocampal output pathway (Ohara et al., 2018). However, the chance of finding functional connections between LVa and LVb neurons in paired recordings was fairly low (∼3% in both directions; Fig. 6A), indicating signal processing in two parallel streams. We then tested for recurrent connections within both cell types. Cross-connectivity of neurons within LVb was 5.9% ($n = 51$; Fig. 6B). In contrast, reciprocal connectivity between LVa neurons was rather high (15.6%; $n = 64$; Fig. 6C).

LV FS interneurons in the mEC are activated by hippocampal SPW-Rs (see above). We next asked whether they also receive excitatory input from glutamatergic neurons within mEC LV and whether they mediate SPW-R-driven inhibition of LVa and LVb excitatory cells. Indeed, paired recordings between FS interneurons and excitatory neurons revealed that they receive excitatory synaptic input from both LVa and LVb cells. However, the success rate for input from LVa neurons to FS interneurons was substantially higher (50%; $n = 26$) when compared with connections from LVb neurons (5%; $n = 40$; $p < 0.001$, Fisher's exact test). Furthermore, the connectivity between LVa neurons and FS interneurons was asymmetric: excitatory connections from LVa to FS were more frequent than inhibitory connections from FS to LVa (Fig. 6D; $p = 0.027$, Fisher's exact test). This relation between excitatory and inhibitory connections was opposite to that between LVb and FS neurons (Fig. 6E; $p < 0.001$, Fisher's exact test). A direct comparison revealed that LVb cells were apparently more frequently inhibited by FS interneurons than LVa cells (FS to LVb: 36.6%; $n = 41$; FS to LVa: 20.7%; $n = 29$; Fig. 6D,E). This apparent difference, however, did not reach significance ($p = 0.191$, Fisher's exact test). We also analyzed whether response amplitudes depended on the distance between the recorded neurons (Fig. 6). In most types of connections, we did not see such dependence within the range of our recordings (∼80 to 120 μm). Connections from FS neurons to LVa neurons, however, showed a significant negative correlation between PSP amplitude and distance.

In brief, we found the following properties of the mEC layer V microcircuit: (1) there is very limited synaptic

interaction between LVb and LVa excitatory neurons; (2) layer Vb neurons are recurrently connected at rates of <10%, a typical value for pyramidal cells in other cortical regions; (3) LVa neurons are more frequently interconnected (~16%); and (4) FS interneurons receive a major local excitatory input that comes preferentially from LVa cells.

SPW-R-driven inhibition of LVa and LVb neurons

How does the natural activity pattern of SPW-Rs affect the different neuronal subtypes in mEC layer V? To assess the relation between SPW-R-driven excitation and inhibition of LVa and LVb cells, we measured EPSCs and IPSCs separately (Fig. 7A). EPSCs were recorded at a holding potential (V_h) corresponding to E_{GABA-A} (approximately -90 mV) and IPSCs at around E_{AMPA} (0 mV). In these experiments, V_h was corrected for liquid junction potential. To improve space-clamp conditions, we used a cesium-based internal solution ("low CsCl") containing 4 mM Cl$^-$. Similar to recordings of mixed PSPs, spontaneous SPW-Rs triggered EPSCs significantly more frequently in LVa neurons (86%; $n = 12$) than in LVb pyramidal cells (53%; $n = 12$; $p = 0.0005$, Wilcoxon test; Fig. 7B). Cross-correlation analysis showed higher peak values for LVa neurons compared with LVb neurons ($p = 0.011$, Mann–Whitney test; z-score: for LVa: 30.4 (13.8; 48.7); for LVb: 15.7 (3.3; 20.7)). While latencies of EPSCs were not significantly different between LVa neurons (12.6 ms; $n = 12$) and LVb neurons (19.9 ms; $n = 12$; $p = 0.064$, Wilcoxon test; Fig. 7D), median EPSC amplitudes were higher in LVa than in LVb neurons (LVa: -55 pA; LVb: -20 pA; $n = 12$; $p = 0.0005$). The events were also longer in duration in LVa than in LVb neurons (LVa: 22.7 ms; LVb: 15.1 ms; $n = 12$; $p = 0.0024$) and mediated a larger charge transfer, calculated as current–time integrals (LVa: 0.80 pC; LVb: 0.17 pC; $n = 12$; $p = 0.0005$, for all Wilcoxon tests; Fig. 7D,F). Thus, our data suggest that LVa neurons receive more reliable and significantly stronger excitatory drive during SPW-Rs than LVb pyramidal cells. In contrast to EPSCs, the occurrence of SPW-R-associated IPSCs in both cell populations was nearly identical (LVa: 22%; LVb: 17%, $n = 12$; $p = 0.203$; Fig. 7C). In paired recordings from LVa and LVb neurons, parameters of inhibitory currents were largely similar (LVa vs LVb): propagation latencies were 21.5 versus 22.5 ms ($n = 11$, $p = 0.966$); IPSC amplitude was 28.7 versus 24.0 pA ($n = 12$, $p = 0.052$); IPSC duration was 31.4 versus
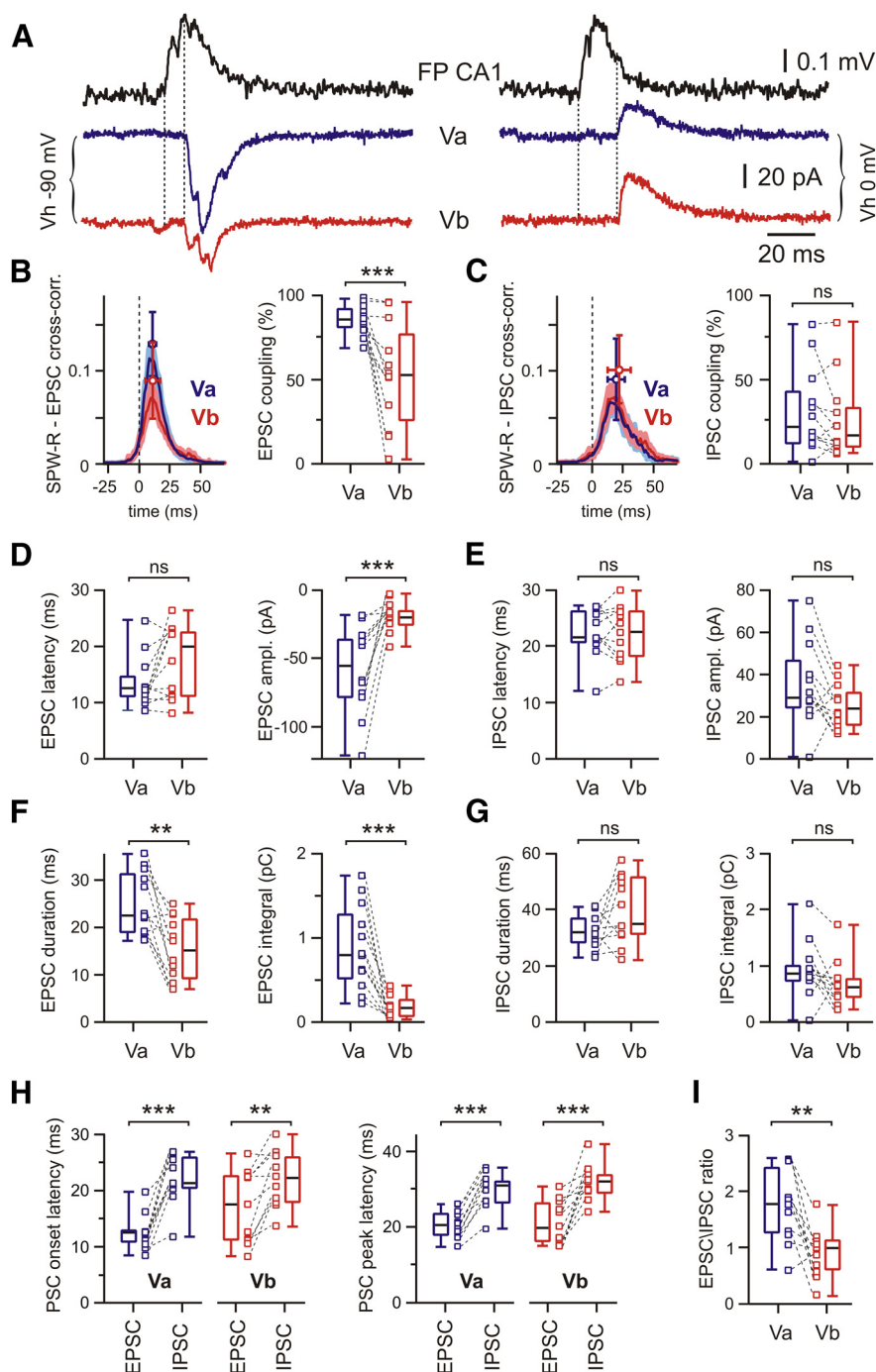

Figure 7. Postsynaptic currents in mEC LVa and LVb neurons during SPW-R activity. **A**, Raw traces of SPW-Rs recorded in CA1 and associated PSCs recorded from mEC LVa and LVb neurons at two different holding potentials highlighting putative EPSCs (left) and IPSCs (right). Dotted lines indicate PSC latency. **B**, Averaged cross-correlograms between SPW-Rs and EPSCs in LVa (blue) and LVb (red) neurons (peak values: mean ± SD; left). Box plots show higher EPSC coupling to SPW-Rs for LVa compared with LVb neurons (right). **C**, Same analysis as in **B** for IPSCs. No difference between LVa and LVb neurons for inhibitory coupling to SPW-Rs. **D**, Box plots of EPSC latency and amplitude for LVa and LVb neurons. **E**, Latency and amplitude of IPSCs. **F**, Box plots of EPSC duration and charge transfer (current integral) for LVa and LVb neurons. Note the stronger input to LVa neurons compared with LVb neurons. **G**, Same as in **F** for IPSCs. **H**, Latency of PSC onset (left) and peak (right) for both cell populations and response directions. IPSC latency is significantly longer than EPSC latency for both types of excitatory LV neurons. **I**, EPSC/IPSC amplitude ratios. Note the stronger net excitation of LVa versus LVb neurons. Data are presented as the median (P_{25}; P_{75}) and individual values. Whiskers show minimum and maximum values. Wilcoxon test: **$p < 0.01$; ***$p < 0.001$; ns, not significant.

34.2 ms ($n = 11$, $p = 0.083$); and IPSC integrals were 0.85 versus 0.62 pC ($n = 12$, $p = 0.110$, Wilcoxon test for all parameters; Fig. 7E,G). Latency of IPSCs was significantly longer compared with EPSCs for both types of excitatory LV neurons (Fig. 7H). As a

result of this analysis, the EPSC/IPSC amplitude ratio of responses elicited by SPW-Rs was significantly higher in LVa neurons than in LVb neurons (1.8 vs 1.0; $n = 11$; $p = 0.005$, Wilcoxon test; Fig. 7I).

Discussion

We investigated the processing of evoked and naturally occurring hippocampal activity patterns in the mouse entorhinal cortex. We show that stimulation of hippocampal outputs at intermediate/ventral levels directly excites both types of glutamatergic cells in mEC layer V (LVb and LVa neurons) as well as fast-spiking inhibitory interneurons. Connections between LVb and LVa neurons are very sparse, indicating that hippocampal inputs are split into two parallel streams of activity in the receiving layers of the mEC. Of note, this configuration minimizes the influence of LVb cells on information transfer to telencephalic structures, which is likely mediated by LVa neurons. Finally, excitation by propagating sharp wave–ripple complexes is stronger in LVa cells than in LVb cells, indicating preferential routing of SPW-R-encoded information to remote neocortical networks, rather than circulating activity within the entorhinal–hippocampal loop.

Direct functional hippocampal projection to mEC LVa neurons

Layer V of the mEC receives a substantial part of the output from hippocampal networks and might thus be involved in transferring temporally stored hippocampal information to downstream neocortical networks for long-term memory formation (Roy et al., 2017). The receiving layer of the mEC, layer V, has recently been demonstrated to be divided into two major sublayers, termed Va and Vb, respectively (Sürmeli et al., 2015). LVa neurons are the major source of telencephalic projections, including the retrosplenial cortex (RSC), prelimbic cortex, nucleus accumbens (NAc), and basolateral amygdala (Sürmeli et al., 2015; Ohara et al., 2018). In contrast, LVb neurons give rise to local connections within the mEC by sending axons to hippocampal-projecting neurons of LII and LIII as well as toward LVa (Ohara et al., 2018). Our present results demonstrate that the intermediate/ventral hippocampus sends direct excitatory input to both major glutamatergic neurons of mEC LV. The natural "output" pattern of hippocampal networks, SPW-R (Chrobak and Buzsáki, 1996), caused clear synaptic responses in LVa neurons, which were even more reliable than those in LVb. Responses persisted in a modified extracellular solution favoring monosynaptic transmission, and delay times were similar between LVa and LVb neurons in all experimental conditions (SPW-Rs, electrical, or optogenetic stimulation). These findings suggest strong monosynaptic connections between CA1 and LVa neurons, similar to LVb neurons.

Previous work has revealed a lack of direct projections from the hippocampus to LVa neurons, based on the distribution of labeled terminals in the mEC and on functional tests of connectivity (Sürmeli et al., 2015; Ohara et al., 2018). These studies, however, tested projections from the dorsal portion of the hippocampus to the mEC, while the present work focused on interactions at intermediate/ventral levels. To compare these different approaches, we performed additional recordings following ChR2-expressing AAV injections into the dorsal hippocampus. While we found monosynaptic responses in ~65% of all tested LVa neurons, these responses were clearly weaker than those in LVb cells. At the structural level, this difference coincides with a much stronger projection of dorsal hippocampal axons to LVb compared with LVa.
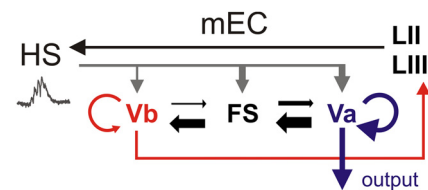

Figure 8. Two distinct pathways for processing hippocampal network activity in the receiver network of the mEC LV. Schematic representation of internal and external connections of mEC layer V at the intermediate/ventral level of the hippocampus (HS). SPW-Rs directly excite both LVb and LVa neurons, as well as FS inhibitory interneurons. Layer Vb neurons constitute a local circuit element projecting to layers II and III, which close the entorhinal–hippocampal loop. In contrast, LVa neurons are the major source of intratelencephalic projections. Connections between LVb and LVa excitatory neurons are sparse, suggesting that hippocampal output signals are split into two parallel streams of activity in the entorhinal cortex. Layer Vb neurons are reciprocally connected at rates of ~6%, typical for pyramidal cells. LVa excitatory neurons are interconnected more frequently (~16%), suggesting the functional amplification of mEC output signals. FS interneurons receive stronger local excitatory input from LVa than LVb excitatory cells. Asymmetric internal connections in layer V suggest preferential inhibition of LVb neurons. During SPW-Rs, net excitation is stronger for LVa neurons than for LVb cells, indicating a preference for the output of SPW-R activity to telencephalic structures over signal propagation within the entorhinal cortex.

Our data on projections originating from the dorsal hippocampus are thus in general agreement with those from the study by Sürmeli et al. (2015), showing a clear preference for excitation of LVb over LVa neurons. In contrast, at intermediate/ventral levels, stimulation-induced responses are far more symmetrical. Such differences along the dorsoventral–hippocampal axis have been shown in numerous studies (Strange et al., 2014), including different connections with cortical and subcortical areas (Cenquizca and Swanson, 2007), diverse patterns of gene expression (Cembrowski et al., 2016), spread of ripple activity (Patel et al., 2013), and spatial encoding (Kjelstrup et al., 2008).

Functional connectivity within mEC LV

Paired recordings revealed characteristic features of functional connectivity within the mEC layer V network. First, functional connections between glutamatergic neurons in LVb and LVa are sparse (~3%). Thus, there is only limited direct excitatory cross talk between the two sublayers. This seems to be in contrast with anatomical data based on transsynaptic rabies virus-mediated tracing, which indicates substantial connections between mEC neurons in layer Vb and NAc/RSC-projecting LVa neurons (Ohara et al., 2018). Possibly, some of the anatomically demonstrated connections involve inhibitory interneurons in layer Vb, which, according to our paired recordings, are clearly connected with horizontal neurons in layer Va (20.7%). Second, recurrent connections within sublayers are more frequent for LVa–LVa pairs (15.6%) than for LVb–LVb pairs (5.9%). Layer Va neurons form the main source of telencephalic projections. The strong interconnections between these cells may thus form an excitatory loop for functional amplification of mEC output signals. Third, fast-spiking interneurons in layer V receive more innervation from LVa than from LVb neurons. As a result, connectivity within the mEC layer V micronetwork suggests preferential activation of Va neurons and inhibition of Vb neurons. This connectivity would favor excitation of telencephalic target regions (LVa) rather than backpropagation of activity into the entorhinal–hippocampal loop (LVb; Fig. 8).

Propagation of hippocampal SPW-R oscillations to mEC LV

Hippocampal SPW-R oscillations propagate reliably to the deep layers of mEC, mainly LV (Chrobak and Buzsáki, 1996; Isomura

et al., 2006; Roth et al., 2016; Gardner et al., 2019). Recently, coordinated replay of activity patterns between CA1 and the deep layers of the mEC has been suggested (Ólafsdóttir et al., 2016, 2017). These studies establish an intricate functional connection between the hippocampus proper and mEC layer V but leave open how afferent signals are processed within this micronetwork. Our assessment of synaptic connections toward and between the major cell types of mEC LV suggests that, at the intermediate/ventral topographic level, hippocampal output signals activate two parallel pathways. One branch goes via LVb neurons to superficial layers of the mEC, which form projections back to the hippocampus (Ohara et al., 2018). This recurrent loop may be functionally important (e.g., for stabilizing patterned neuronal activity during active network states). In line with this notion, mEC LIII input to CA1 has been shown to be critical for ripple bursts and long-range replay of activity patterns, at least in certain vigilance states (Yamamoto and Tonegawa, 2017). The other pathway involves horizontal neurons in LVa that project to telencephalic areas. This output may be instrumental for instructing downstream neocortical networks, which may serve memory consolidation (Khodagholy et al., 2017; Kitamura et al., 2017; Wilber et al., 2017). Our recordings suggest that the far-projecting pathway constituted by layer Va neurons may be particularly strong, as supported by their intense recurrent connectivity and high excitation/inhibition ratio compared with LVb neurons. This is in line with the supposed role of the deep layers of the mEC, which mostly support output functions during the "offline" mode of the hippocampus (Buzsáki, 2015).

Ripple episodes occur along the full extension of the hippocampal CA1 region. At different levels, however, they show characteristic differences in their intrahippocampal propagation patterns (Patel et al., 2013), which may be related to the different information content and connectivity along the dorsoventral axis (Swanson and Cowan, 1977; van Groen and Wyss, 1990; Strange et al., 2014; Laventure and Benchenane, 2020). We note that, with respect to network activity, our present study focuses on intermediate/ventral hippocampal–entorhinal connections. We also note that we recorded from the medial EC. Functional connectivity may be different in the lEC, which has different cortical interactions and behavioral-cognitive functions (Witter et al., 2017; Tsao et al., 2018; Nilssen et al., 2019).

Another important finding of this study is that FS layer V interneurons are strongly excited by hippocampal network activity. Afferent SPW-Rs caused excitatory postsynaptic potentials in FS neurons with >90% reliability and with higher amplitudes than in both types of glutamatergic cells. Since LTS interneurons showed no synchronized activity during hippocampal SPW-Rs, it is likely that FS interneurons are the main source of inhibition for LVb and LVa neurons for this type of propagating network. Voltage-clamp experiments did not reveal a difference in the strength of inhibition between both excitatory cell types during SPW-Rs. However, analysis of intra-mEC connections by paired recordings revealed an asymmetry in local innervation of LVa and LVb cells, respectively, favoring excitation of LVa and inhibition of LVb cells. The reasons for this discrepancy are presently unclear and may involve state-dependent differences in the recruitment of FS interneurons (Csicsvari et al., 1999; Buzsáki and Wang, 2012; Butler and Paulsen, 2015). Nevertheless, our data reveal a clear prevalence for excitation of LVa over LVb neurons during SPW-Rs: excitatory postsynaptic currents are stronger in LVa than in LVb cells; and coupling of PSPs with SPW-R events is more abundant for LVa cells than for LVb cells. Together, these findings indicate that SPW-R activity from the intermediate/ventral hippocampus is preferentially passed via LVa neurons to telencephalic structures, while the feedback loop to the hippocampus via LVb neurons is less strongly activated (Fig. 8). This preference may be different in different neuromodulatory/behavioral states (e.g., during wakefulness; Yamamoto and Tonegawa, 2017).

In summary, our data reveal that the deep layers of the mEC act as a bifurcation gate for hippocampal network activity. Both connectivity data and recordings of native network activity indicate robust innervation of LVa and LVb neurons from the intermediate/ventral hippocampus, with stronger excitation of telencephalic projecting LVa cells. These findings suggest a new model for the entorhinal cortex, which relays hippocampal activity into two parallel pathways and supports efficient hippocampal–neocortical dialogue.

References

Bressler SL, Menon V (2010) Large-scale brain networks in cognition: emerging methods and principles. Trends Cogn Sci 14:277–290.

Butler JL, Paulsen O (2015) Hippocampal network oscillations - recent insights from in vitro experiments. Curr Opin Neurobiol 31:40–44.

Buzsáki G (1986) Hippocampal sharp waves: their origin and significance. Brain Res 398:242–252.

Buzsáki G (1989) Two-stage model of memory trace formation: a role for "noisy" brain states. Neuroscience 31:551–570.

Buzsáki G (2015) Hippocampal sharp wave-ripple: a cognitive biomarker for episodic memory and planning. Hippocampus 25:1073–1188.

Buzsáki G, Moser EI (2013) Memory, navigation and theta rhythm in the hippocampal-entorhinal system. Nat Neurosci 16:130–138.

Buzsáki G, Wang XJ (2012) Mechanisms of gamma oscillations. Annu Rev Neurosci 35:203–225.

Canto CB, Witter MP (2012) Cellular properties of principal neurons in the rat entorhinal cortex. II. The medial entorhinal cortex. Hippocampus 22:1277–1299.

Cembrowski MS, Bachman JL, Wang L, Sugino K, Shields BC, Spruston N (2016) Spatial gene-expression gradients underlie prominent heterogeneity of CA1 pyramidal neurons. Neuron 89:351–368.

Cenquizca LA, Swanson LW (2007) Spatial organization of direct hippocampal field CA1 axonal projections to the rest of the cerebral cortex. Brain Res Rev 56:1–26.

Chrobak JJ, Buzsáki G (1996) High-frequency oscillations in the output networks of the hippocampal-entorhinal axis of the freely behaving rat. J Neurosci 16:3056–3066.

Chrobak JJ, Buzsáki G (1998) Gamma oscillations in the entorhinal cortex of the freely behaving rat. J Neurosci 18:388–398.

Csicsvari J, Hirase H, Czurkó A, Mamiya A, Buzsáki G (1999) Oscillatory coupling of hippocampal pyramidal cells and interneurons in the behaving rat. J Neurosci 19:274–287.

Egorov AV, Heinemann U, Müller W (2002) Differential excitability and voltage-dependent Ca2+ signalling in two types of medial entorhinal cortex layer V neurons. Eur J Neurosci 16:1305–1312.

Fuster JM (2006) The cognit: a network model of cortical representation. Int J Psychophysiol 60:125–132.

Gardner RJ, Lu L, Wernle T, Moser MB, Moser EI (2019) Correlation structure of grid cells is preserved during sleep. Nat Neurosci 22:598–608.

Girardeau G, Benchenane K, Wiener SI, Buzsáki G, Zugaro MB (2009) Selective suppression of hippocampal ripples impairs spatial memory. Nat Neurosci 12:1222–1223.

Gray CM, Singer W (1989) Stimulus-specific neuronal oscillations in orientation columns of cat visual cortex. Proc Natl Acad Sci U S A 86:1698–1702.

Haas HL, Schaerer B, Vosmansky M (1979) A simple perfusion chamber for the study of nervous tissue slices in vitro. J Neurosci Methods 1:323–325.

Hájos N, Ellender TJ, Zemankovics R, Mann EO, Exley R, Cragg SJ, Freund TF, Paulsen O (2009) Maintaining network activity in submerged hippocampal slices: importance of oxygen supply. Eur J Neurosci 29:319–327.

Hamam BN, Kennedy TE, Alonso A, Amaral DG (2000) Morphological and electrophysiological characteristics of layer V neurons of the rat medial entorhinal cortex. J Comp Neurol 418:457–472.

Isomura Y, Sirota A, Ozen S, Montgomery S, Mizuseki K, Henze DA, Buzsáki G (2006) Integration and segregation of activity in entorhinal-hippocampal subregions by neocortical slow oscillations. Neuron 52:871–882.

Khodagholy D, Gelinas JN, Buzsáki G (2017) Learning-enhanced coupling between ripple oscillations in association cortices and hippocampus. Science 358:369–372.

Kitamura T, Ogawa SK, Roy DS, Okuyama T, Morrissey MD, Smith LM, Redondo RL, Tonegawa S (2017) Engrams and circuits crucial for systems consolidation of a memory. Science 356:73–78.

Kjelstrup KB, Solstad T, Brun VH, Hafting T, Leutgeb S, Witter MP, Moser EI, Moser MB (2008) Finite scale of spatial representation in the hippocampus. Science 321:140–143.

Kumar A, Rotter S, Aertsen A (2010) Spiking activity propagation in neuronal networks: reconciling different perspectives on neural coding. Nat Rev Neurosci 11:615–627.

Laventure S, Benchenane K (2020) Validating the theoretical bases of sleep reactivation during sharp-wave ripples and their association with emotional valence. Hippocampus 30:19–27.

Liao X, Walters ET (2002) The use of elevated divalent cation solutions to isolate monosynaptic components of sensorimotor connections in aplysia. J Neurosci Methods 120:45–54.

Maier N, Nimmrich V, Draguhn A (2003) Cellular and network mechanisms underlying spontaneous sharp wave-ripple complexes in mouse hippocampal slices. J Physiol 550:873–887.

McLean HA, Caillard O, Khazipov R, Ben-Ari Y, Gaiarsa JL (1996) Spontaneous release of GABA activates GABAB receptors and controls network activity in the neonatal rat hippocampus. J Neurophysiol 76:1036–1046.

Nakashiba T, Buhl DL, McHugh TJ, Tonegawa S (2009) Hippocampal CA3 output is crucial for ripple-associated reactivation and consolidation of memory. Neuron 62:781–787.

Nilssen ES, Doan TP, Nigro MJ, Ohara S, Witter MP (2019) Neurons and networks in the entorhinal cortex: a reappraisal of the lateral and medial entorhinal subdivisions mediating parallel cortical pathways. Hippocampus 29:1238–1254.

Ohara S, Onodera M, Simonsen ØW, Yoshino R, Hioki H, Iijima T, Tsutsui KI, Witter MP (2018) Intrinsic projections of layer Vb neurons to layers Va, III, and II in the lateral and medial entorhinal cortex of the rat. Cell Rep 24:107–116.

Ólafsdóttir HF, Carpenter F, Barry C (2016) Coordinated grid and place cell replay during rest. Nat Neurosci 19:792–794.

Ólafsdóttir HF, Carpenter F, Barry C (2017) Task demands predict a dynamic switch in the content of awake hippocampal replay. Neuron 96:925–935. e6.

Patel J, Schomburg EW, Berényi A, Fujisawa S, Buzsáki G (2013) Local generation and propagation of ripples along the septotemporal axis of the hippocampus. J Neurosci 33:17029–17041.

Paxinos G, Franklin KBJ (2001) The mouse brain in stereotaxic coordinates, Ed 2. San Diego: Academic.

Roth FC, Beyer KM, Both M, Draguhn A, Egorov AV (2016) Downstream effects of hippocampal sharp wave ripple oscillations on medial entorhinal cortex layer V neurons in vitro. Hippocampus 26:1493–1508.

Roy DS, Kitamura T, Okuyama T, Ogawa SK, Sun C, Obata Y, Yoshiki A, Tonegawa S (2017) Distinct neural circuits for the formation and retrieval of episodic memories. Cell 170:1000–1012.

Seidenbecher T, Laxmi TR, Stork O, Pape H-C (2003) Amygdalar and hippocampal theta rhythm synchronization during fear memory retrieval. Science 301:846–850.

Siapas AG, Wilson MA (1998) Coordinated interactions between hippocampal ripples and cortical spindles during slow-wave sleep. Neuron 21:1123–1128.

Squire LR, Genzel L, Wixted JT, Morris RG (2015) Memory consolidation. Cold Spring Harb Perspect Biol 7:a021766.

Strange BA, Witter MP, Lein ES, Moser EI (2014) Functional organization of the hippocampal longitudinal axis. Nat Rev Neurosci 15:655–669.

Sürmeli G, Marcu DC, McClure C, Garden DLF, Pastoll H, Nolan MF (2015) Molecularly defined circuitry reveals input-output segregation in deep layers of the medial entorhinal cortex. Neuron 88:1040–1053.

Swanson LW, Cowan WM (1977) An autoradiographic study of the organization of the efferent connections of the hippocampal formation in the rat. J Comp Neurol 172:49–84.

Tsao A, Sugar J, Lu L, Wang C, Knierim JJ, Moser MB, Moser EI (2018) Integrating time from experience in the lateral entorhinal cortex. Nature 561:57–62.

Valeeva G, Janackova S, Nasretdinov A, Rychkova V, Makarov R, Holmes GL, Khazipov R, Lenck-Santini PP (2019) Emergence of coordinated activity in the developing entorhinal-hippocampal network. Cereb Cortex 29:906–920.

van Groen T, Wyss JM (1990) Extrinsic projections from area CA1 of the rat hippocampus: olfactory, cortical, subcortical, and bilateral hippocampal formation projections. J Comp Neurol 302:515–528.

van Strien NM, Cappaert NLM, Witter MP (2009) The anatomy of memory: an interactive overview of the parahippocampal-hippocampal network. Nat Rev Neurosci 10:272–282.

Wilber AA, Skelin I, Wu W, McNaughton BL (2017) Laminar organization of encoding and memory reactivation in the parietal cortex. Neuron 95:1406–1419.

Witter MP, Doan TP, Jacobsen B, Nilssen ES, Ohara S (2017) Architecture of the entorhinal cortex a review of entorhinal anatomy in rodents with some comparative notes. Front Syst Neurosci 28:11–46.

Yamamoto J, Tonegawa S (2017) Direct medial entorhinal cortex input to hippocampal CA1 is crucial for extended quiet awake replay. Neuron 96:217–227.